

Catalysis Science & Technology

Accepted Manuscript



This is an *Accepted Manuscript*, which has been through the Royal Society of Chemistry peer review process and has been accepted for publication.

Accepted Manuscripts are published online shortly after acceptance, before technical editing, formatting and proof reading. Using this free service, authors can make their results available to the community, in citable form, before we publish the edited article. We will replace this *Accepted Manuscript* with the edited and formatted *Advance Article* as soon as it is available.

You can find more information about *Accepted Manuscripts* in the [Information for Authors](#).

Please note that technical editing may introduce minor changes to the text and/or graphics, which may alter content. The journal's standard [Terms & Conditions](#) and the [Ethical guidelines](#) still apply. In no event shall the Royal Society of Chemistry be held responsible for any errors or omissions in this *Accepted Manuscript* or any consequences arising from the use of any information it contains.

Palladium nanoparticles confined in thiol-functionalized ordered mesoporous silica for more stable Heck and Suzuki catalysts.

Cite this: DOI: 10.1039/x0xx00000x

Received 00th January 2012,
Accepted 00th January 2012

DOI: 10.1039/x0xx00000x

www.rsc.org/

Rafael L. Oliveira,^a Wuliyasu He^a, Robertus J. M. Klein Gebbink^b, Krijn P. de Jong^{*a}

Palladium nanoparticles of similar size of ~2 nm were synthesized on different silica-based materials all functionalized with thiol groups i.e., Aerosil-380, SBA-15, Plugged SBA-15 and m-MCF. The resulting materials were used to study the influence of confinement of Pd nanoparticles in functionalized silica support on the Heck and the Suzuki reaction. In the case of the Heck reaction, for all catalysts it was proven that leached Pd species were responsible for activity. However, the catalysts based on ordered mesoporous silica were still able to restrict Pd particle growth giving rise to an enhanced stability. For the Suzuki reaction, stronger alkaline conditions were required and catalysts based on plugged SBA-15 showed a higher stability than those based on SBA-15 and m-MCF which both collapsed after the first cycle. At almost identical Pd particle size, ordered mesoporous materials enhance stability and particle growth is slowed down but not fully suppressed.

Introduction

Ordered mesoporous silica (OMS) such as SBA-15 and MCM-41 has attracted increased interest in the last two decades because of their unique properties such as controllable pore size, large internal surface area and narrow pore size distribution. Due to these properties, numerous applications of OMS in different fields have been reported such as sensors¹⁻³, drug delivery systems⁴⁻⁶, chromatography^{7,8} and catalysis⁹⁻¹⁶. In catalysis, however, siliceous materials do not have sufficient intrinsic activity and a lot of effort has been done to introduce active species in their pores such as organometallic complexes, molecules with alkaline and acidic properties and metal particles.¹⁷⁻²⁰

Silica has been used as support to many different metal nanoparticles.²¹⁻²⁶ However, OMS has been shown very interesting because of the possibility to study the effect of confinement of nanoparticles on their stability. Hao et al. compared the catalytic activity of gold nanoparticles immobilized on SBA-16 and commercial silica gel on the oxidative esterification of alcohols, concluding that the cages of SBA-16 were efficient to prevent the growth of Au, as consequence Au/SBA-16 showed a longer life time.²⁷ Prieto et al. observed the same phenomena for methanol synthesis using Zn promoted Cu nanoparticles immobilized in SBA-16 and silica gel.²⁸ In another example, Sun et al. proved that silver

nanoparticles confined in SBA-15 have a higher thermal stability than particles immobilized on silica gel surface.²⁹

Despite the vast literature about mesoporous materials in catalysis, these materials face big limitations, i.e.s their limited mechanical and hydrothermal stability. Many efforts have been done to produce OMS with a higher stability, for example, Kisler et al. functionalized MCM-41 surface with alkyl groups and proved that its hydrothermal stability increased significantly.³⁰ Pham et al. coated SBA-15 structure with a thin carbon film and reported that the synthesized material has a higher hydrothermal stability than SBA-15.³¹ Van der Voort et al. modified the SBA-15 synthesis and produced a new material called plugged SBA-15, this material showed a higher mechanical and a thermal stability when compared to other OMS, due to the pillaring effect.³²⁻³⁴

Plugged SBA-15 was synthesized using an excess of tetraethyl orthosilicate (TEOS), the silica precursor, leading to an ordered mesoporous silica with constricted pores. By varying the synthesis parameters, the extent of plugging can be influenced. Further studies on plugged SBA-15 showed that entrance sizes and cavities length can be tuned by changing synthetic parameters.^{35,36} Another interesting OMS is modified mesocellular foam (m-MCF) that was recently synthesized by Shakeri et al.³⁷ The procedure is based on P.SBA-15 synthesis, but in this case they introduced a

swelling agent (mesitylene) during the synthesis which caused the formation of larger cages. A very interesting characteristic of this material is its narrow entrance sizes and large cages. Moreover, they also showed using electron tomography that the cages are connected with 9-12 neighboring cavities resulting in a highly interconnected network.

Palladium nanoparticles have been widely immobilized on different supports and have been applied as catalyst for many reactions such as oxidation, reduction, C-C cross coupling and others,³⁸⁻⁴⁷ among C-C coupling reactions, the Suzuki and the Heck reactions are the most explored examples. However, Pd nanoparticles immobilized on inorganic matrixes often suffer from leaching and particle growth due to Ostwald ripening, resulting in a limited recyclability in most cases⁴⁸⁻⁵¹ Recently, a lot of work has been done to produce more efficient heterogeneous catalysts for C-C cross coupling reactions. For examples, Pagliaro et al. entrapped Pd nanoparticles using a sol-gel procedure, producing leach-proof nanostructures; these materials could be recycled seven times without losing activity.⁵² Budroni et al. also entrapped Pd nanoparticles in a sponge-like silica and reported that leached species were partially responsible for the conversion.⁵³ Park et al. immobilized Pd nanoparticles in silica nanotubes producing efficient nano-reactors for the Suzuki reaction, and they reported an insignificant Pd leaching and concluded the surface nature of the Suzuki reaction.⁵⁴

A lot of reports in literature have shown that supports with functional groups containing sulfur, nitrogen, phosphorous can lead to more stable catalysts for C-C cross coupling.⁵⁵⁻⁶¹ Recently, our group reported that SBA-15 with thiol grafted on its surface produced a more stable catalyst than Pd immobilized on bare SBA-15.⁶² In another example, Ma et al. used an ionic liquid to stabilized palladium nanoparticles on SBA-15 surface. They reported a higher stability of this material when compared with Pd impregnated on pristine SBA-15.⁶³

In this contribution, Pd nanoparticles of the almost the same size were synthesized on different silica supports, i.e., Aerosil-380, SBA-15, Plugged SBA-15, m-MCF all modified with thiol ligands. These materials were used to study the effect of the confinement of functionalized silica on the activity and the recyclability of the Heck and the Suzuki reaction. The leaching of Pd, growth of Pd particles and the stability of silica supports were examined to explain possible reasons for deactivation of the catalysts.

EXPERIMENTAL

Synthesis and catalytic performance

Chemicals

Triblock copolymer poly(ethylene oxide)-poly(propylene oxide)-poly(ethylene oxide) (P123), tetraethyl orthosilicate 99%, (3-mercaptopropyl)-triethoxysilane 80%, 2% cross-linked poly(4-vinylpyridine) (PVPy), butyl acrylate 99%, triethylamine 99%,

tetraamminepalladium(II) nitrate solution 10w/w% in water and 5wt % Pd on Carbon (product number 20568-0) were purchased from Sigma-Aldrich. Palladium acetate (Pd(OAc)₂, 47.1% Pd) and Aerosil-380 were purchased from Degussa and iodobenzene 98%, 4-iodoanisole 98% and n-butylamine 99% were purchased from Acros Organics

Ordered Mesoporous Silica

SBA-15 and plugged SBA-15 (hereafter referred to as P-SBA-15) were synthesized following a procedure previously described.³⁶

For m-MCF synthesis, 4 grams of copolymer Pluronic P123 was dissolved in an aqueous acidic solution (150 ml; 1.6 M) in a 500 mL polypropylene bottle at room temperature overnight. Then, 3 grams of TMB (mesitylene) was added to the reaction mixture at 35 °C dropwise and stirred vigorously during 2 h. After this period, 17 grams of TEOS was slowly added to the mixture (1.5mL.min⁻¹) and stirred vigorously during 5 minutes. After this period, the mixture was kept under static condition at 35°C for 20 hours followed by 24 hours at 80°C. The solid product was collected by filtration, washed with distilled water, dried at 60°C during 24h and calcined at 550°C in static air during 6 hours.

Functionalization of silica surface

500 mg of SBA-15, P-SBA-15, m-MCF and aerosil-380 was dried at 140°C under vacuum during 12 hours. After this, the solid was dispersed in 20mL of dried toluene under nitrogen. Then, 2.0 mL of (3-thiopropyl)triethoxysilane (MPTES) was added to the mixture dropwise over 5 minutes under vigorous stirring. Then, the mixture was heated at 110°C and stirred during 24 hours under nitrogen. The obtained materials were filtered off and washed 1 time with toluene, 2 times with ethanol and dried at 60°C during 24 hours.

Aerosil-380 was also functionalized using a different methodology. In this procedure, 500 mg of silica was dried at 140°C as previously described. Then, the silica was dispersed in 20 mL of dried toluene. Then, 300µL glacial CH₃COOH and 1.5 mL of MPTES were added subsequently to the reaction mixture dropwise. The mixture was reacted at 110°C under N₂ for 24 hours. The solid was collected and washed as previously described.

Impregnation of Pd

250 mg of functionalized silica support was dried under vacuum at 140° C during 12 hours. After drying, the solid was dispersed in 5mL dry toluene under N₂. 8mg of palladium(II) acetate was dissolved in 1 mL dichloromethane and then added slowly to the dispersion. The dispersion was then heated to 60°C and stirred during 24h. The solids were collected by centrifugation, washed once with toluene and once with ethanol and finally dried at 60°C. For reduction of palladium, 100mg of Pd-loaded silica was dispersed in 1mL water. Then, 1mL of 0.1M NaBH₄ was added rapidly under vigorous stirring. After 20 minutes, the dispersion was diluted with

water to 35 mL, centrifuged, washed thoroughly with water and dried at 60°C under stagnant air.

Catalyst tests

The Heck reaction

In a typical Heck reaction, a mixed solution of iodobenzene (2.25 mmol), butylacrylate (3.47 mmol), NEt₃(2.15mmol), hexamethylbenzene (internal standard for GC analysis, 1.1mmol) and 2.0 mL of toluene and 0.2 mL of DMF were added to a schlenk, followed by addition of 20 mg of catalyst (0.1 mol% of palladium relative to iodobenzene). Then, the mixture was stirred for a given time and temperature.

After reaction, solid catalysts were recovered by centrifugation and washed with ethanol (35 mL) and dried under vacuum. For recycling experiments, a new solution mixture described above was added to the solid.

The Suzuki reaction

In a typical reaction, a mixed solution of 4-iodoanisole (2.4 mmol), phenylboronic acid (2.88 mmol), base (2.4 mmol,) and solvent (4 mL) were added to a schlenk, followed by addition of 20 mg of catalyst (0.1 mol% of palladium relative to 4-iodoanisole). Then, the mixture was reacted at desired temperature and time. For a recycle experiment, the catalyst was recovered by centrifugation and the solid was washed with ethanol/water (1/1, 2 × 40 mL), ethanol (30 mL) and dried at 60°C overnight. Then, a new solution mixture described above was added to the solid and allows to react during the same period of time. As just one product was observed, the conversions were obtained by external calibration.

GC analysis

A small fraction of the liquid samples were taken and diluted with toluene and analyzed by GC-FID. CG analysis was performed using a PerkinElmer Clarus 500, equipped with a 30m capillary column with 5% phenyl/ 95% methylpolysiloxane as stationary phase(AT5), using the following parameters: initial temperature 50°C, temperature ramp 10°C min⁻¹, final temperature 250°C, injection volume 0.5µL.

Hot filtration test and PVPy poison test

A Heck reaction was allowed to run during 3 hours for a mixture of solvents. Then, the solids were filtered off under static vacuum using a swivel frit filter connected with an empty flask, the filtrate was kept at reaction temperature, the conversion was monitored by GC.

The catalyst poison was added to the Schlenk flask before the addition of reaction solution. Poly(4-vinylpyridine) (2% cross-

linked) (PVPy) was used in 350 equivalents of pyridine sites to total of palladium.

Characterization

Electron Microscopy

The morphology and sizes of the silica particles were determined with a Tecnai FEI XL 30SFEG Scanning Electron Microscope (SEM). Transmission electron microscopy was performed using a microscope FEI Tecnai20F, operated at 200 kV equipped with CCD camera.

The samples were embedded in epoxy resin (Epofix, EMS) and cured at 60°C overnight. Then, they were cut into thin sections with a nominal thickness of 60 nm using a Diatome Ultra knife, 4 mm wide and 35° clearance angle, mounted on a Reichert–Jung Ultracut E microtome. The sections float on water after cutting, were picked up and deposited onto a carbon coated polymer grid and left to dry. The histograms of particle size distribution were obtained from observing about 500 particles in representative micrographs of different areas.

Gas physisorption

N₂ and Ar physisorption measurements were performed at 77 K using a Micromeritics Tristar 3000. The samples were dried before the measurement under a N₂ flow at 250 °C for at least 12 h. The functionalized samples were dried at 130°C during at least 12 h. The total microporous and mesoporous volume (V_p) was determined using the t-plot method. The pore size distribution of the mesoporous silica supports was calculated from the adsorption branch of the isotherm by BJH analysis. The maximum of the pore size distribution was taken as the average pore diameter.

XRD analysis

Long range pore ordering was confirmed with low-angle X-ray diffraction. Patterns were obtained at room temperature from 0.5 to 8° 2θ with a AXS D2 Phaser powder X-ray diffractometer, in Bragg-Brentano mode, equipped with a Lynxeye detector using Co-K_{α12} radiation, with λ = 1.790 Å, operated at 30kV, 10 mA. XRD patterns of palladium were recorded for all solids between 10 and 100° 2θ using the same equipment.

Elemental Analysis

S contents of the silica was determined by Inductively Coupled Plasma-Atomic Emission Spectroscopy (ICP-AES) using a Metrohm IC Plus 883. Pd contents of the solid samples and in the liquids from catalysis experiments were analyzed by Atomic Absorption Spectroscopy (AAS) using an AAS, AANALYST200 Perkin Elmer.

RESULTS AND DISCUSSION

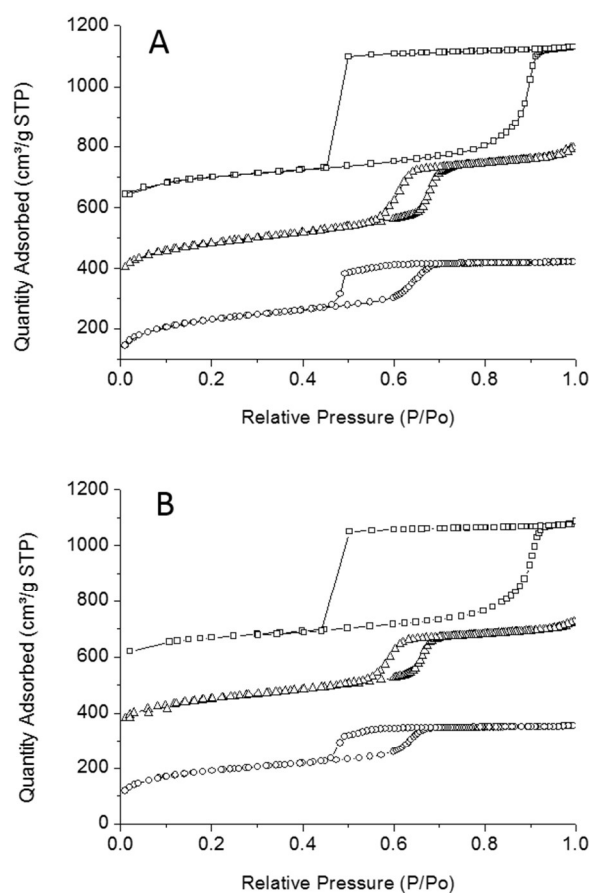
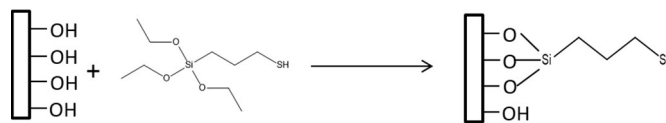


Figure 1 Nitrogen physisorption of ordered mesoporous silica (A) and functionalized ordered mesoporous materials (B) the isotherms were offset by $300\text{cm}^3/\text{g}$ (SBA-15) $500\text{cm}^3/\text{g}$ (m-MCF).

The nitrogen sorption isotherms of the synthesized silica materials are type IV following the IUPAC classification (Figure 1A) since they show one step capillary condensation in the adsorption branch, corresponding to filling of the uniform mesoporous by N_2 molecules. The isotherm shows a typical parallel hysteresis of the open mesopores of SBA-15. In the case of plugged SBA-15, which consists of well-ordered mesoporous silica with constrictions and nanocavities in the pores, N_2 physisorption showed an ink-bottle hysteresis typical for cage-like materials, where desorption is delayed until P/P_0 around 0.47. For m-MCF materials the isotherms showed a broader ink-bottle hysteresis compared to P-SBA-15 confirming the larger cavities inside this material (22 nm in the case of m-MCF and 6 nm for P-SBA-15).

Argon physisorption at 77K is an alternative to study the entrance size of these materials due to the capillary evaporation which happens at lower relative pressures extending its use to analyze smaller entrance sizes. Ar physisorption of plugged SBA-15 and m-MCF (Supporting Information, Figure S1) showed that the entrance size of the cavities had a broad size distribution from 5.6 to 3.6 nm in the case of P-SBA-15 and all entrance sizes were smaller than 3.6 nm for m-MCF.



Scheme 1 Functionalization of silica surface with thiol groups.

Table 1 Structure and composition of silica supported Pd catalysts

Material	Surface area (m^2/g)	Pore Volume (cm^3/g)	S Loading (w/w%)	SH density ($\mu\text{mol}\cdot\text{m}^{-2}$)	Pd loading (w/w%)	S:Pd molar ratio
SiO_2 -SHPd	280	2.32	1.2	1.3	1.48	2.7
SiO_2 -aSHPd	210	1.47	2.5	3.7	1.54	5.4
SBA-15SHPd	660	0.53	2.7	1.3	1.6	5.6
P-SBA-15SHPd	619	0.52	2.43	1.2	1.55	5.2
m-MCF-SHPd	534	0.72	2.61	1.5	1.57	5.5

The thiol groups were grafted on the surface of silica materials using a post synthetic procedure (Scheme 1). Figure 1B shows the isotherms from N_2 physisorption of materials after thiol functionalization. It is observed that functionalized samples displayed a decrease in the specific surface area (Table S1) and pore volume, suggesting functionalization of internal and probably of external walls of OMS materials. The same phenomena were observed for Aerosil samples (designation SiO_2), silica composed by spheres packed together (N_2 physisorption in Figure S2). In the case of SiO_2 , two different methodologies were used (Table 1, designated after Pd loading as SiO_2 SHPd and SiO_2 aSHPd), permitting to obtain materials with different thiol loadings.

SEM images (Figure S3) showed no changes in the morphology after the functionalization procedure. STEM-HAADF analysis (Figure 2) showed that materials kept the same regularity in pore structure. The open pore structure of SBA-15, the constrictions and nanocavities inside plugged SBA-15 and the cages of m-MCF are shown in Figure 2 A, B, C respectively.

After the synthesis of the hybrid supports, palladium was deposited on functionalized silica using a methodology described recently by our group.⁶² TEM analysis (Figure 3) showed that for all cases the structure of silica was unchanged and Pd particles with a very narrow size distribution were observed with an average size of 2.0 ± 0.5 nm. This facilitates the comparison of the catalytic

performance of the materials while excluding the influence of the particle size. Table 1 showed the structural properties of the obtained materials. XRD patterns of the fresh catalysts are shown in Figure S4 showing a very broad peak around $2\theta=50^\circ$ from which we could not derive a crystallite size.

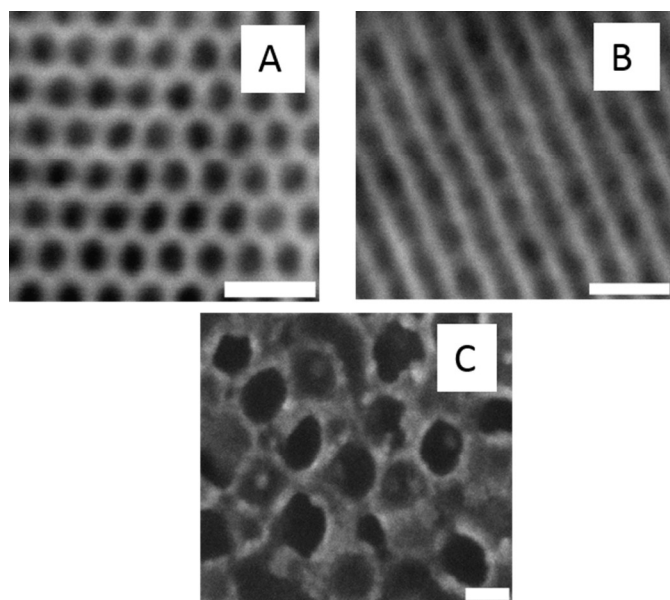


Figure 2 TEM images (A) SBA-15 SH, (B) P. SBA-15 SH and (C) m-MCF SH Scale bars 20nm

The Heck reaction

Table 2 shows the conversion on the Heck reaction between iodobenzene and butyl acrylate (Scheme 2) and the Pd leached after the separation of the catalysts, in all cases butyl cinnamate was the only product formed, the conversion of bromide and chloride substrates are shown in Table S2. All OMS based

catalysts gave rise to similar conversion and metal leaching. However, SiO₂SHPd showed a slightly higher metal leaching. Please note that a mixture of solvents (toluene + DMF) was used as previously reported.⁶²

The loading of thiol groups on the surface of aerosil was increased, permitting it had the same thiol loading and molar ratio between Pd and S as on OMS materials (SiO₂-aSHPd, Table 1). However, this sample showed almost no activity, probably caused by the over-coordination of palladium. As aerosil has a lower specific surface area, the density of thiol per m² was much higher (Table 1), this fact might be causing poisoning of the Pd species. Moreover, Pd leaching was lower for this solid compared to OMS, indicating a stronger interaction between Pd and the ligands on this material. This result is in agreement with an earlier report by Jones et al.,⁶⁴ that an excess of thiol groups was able to poison Pd species, resulting in a loss of the activity on the Heck reaction.

Hot filtration test and PVP test were used to investigate the nature of the reactive species, i.e., surface or leached Pd (Table S3). In all cases, hot filtration showed that leached metal species had a strong influence on the activity for the Heck reaction. Moreover, when PVPy was added, the conversion dropped tremendously confirming the results obtained with the hot filtration tests. This fact might explain why all fresh materials with the same density of thiol displayed almost the same reaction rate (Figure S5, S.I.).

The recyclability of the catalysts are shown in Figure 4, a commercial Pd/C, one of the most used catalyst for these reactions, was also used to compare its stability with synthesized materials. In the case of Pd/C, the catalyst suffered from high metal leaching (20% of original Pd amount), as a consequence no conversion was observed after three cycles, showing a limited stability of this material for the Heck reaction under applied conditions. SiO₂-SHPd started to face a considerable decrease on the activity after four cycles, however, this catalyst showed a higher stability than Pd/C. The solids based on OMS could be used 7 times with only a slight

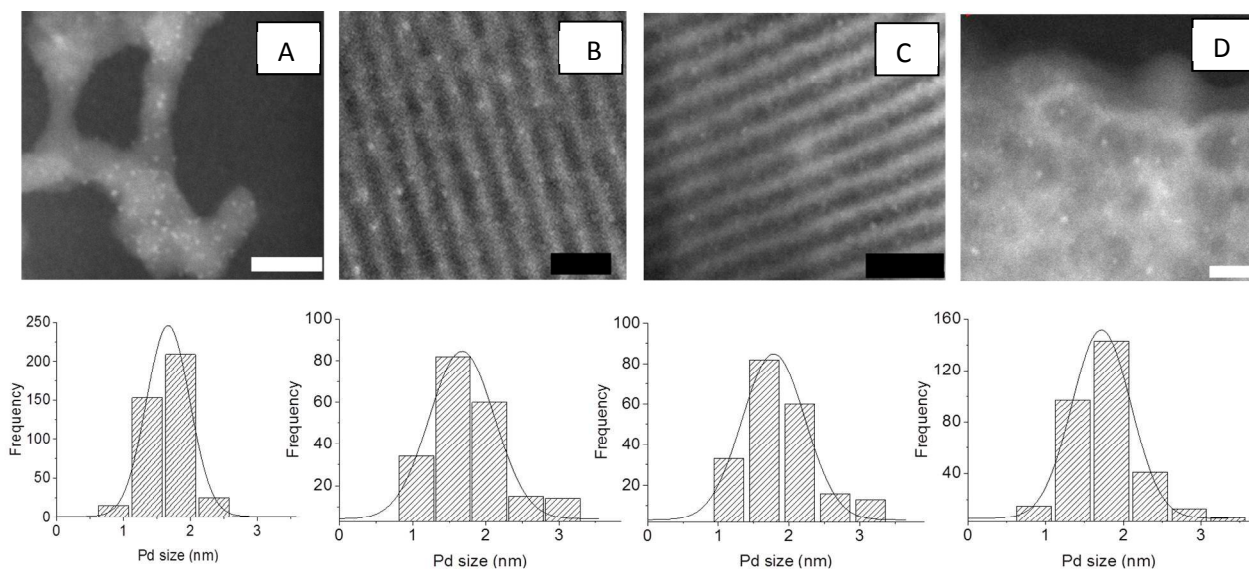
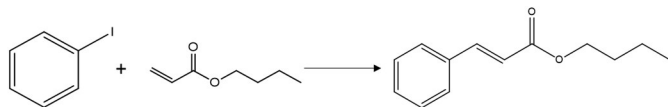


Figure 3 TEM images (A) SiO₂-SHPd (B) SBA-15SHPd (C) P.SBA-15 SHPd (D) m-MCF-SHPd and the corresponding histograms on the bottom. Scale bars are 20 nm



Scheme 2 The Heck reaction between iodobenzene and butyl acrylate

Table 2 The catalytic performance of all synthesized materials and the Pd leaching after the Heck reaction

Samples	Conversion (%)	Pd leaching (%)
SBA-15SHPd	88	0.8
P-SBA-SHPd	88	0.9
m-MCF-SHPd	89	0.7
SiO ₂ -SHPd	85	2.4
SiO ₂ -aSHPd	5	-

Reaction conditions: 2.25 mmol of iodobenzene, 3.4 mmol of butyl acrylate, 20 mg of supported catalyst (0.1 mol% of palladium), 2.14 mmol of Et₃N, 2.0 mL toluene+ 0.2 mL DMF, 100°C, 12 hours reaction time.

reduction of the activity in line earlier publication.⁶² However, here it is shown that Pd in OMS is more stable than Pd on activated carbon or non-porous silica (Aerosil).

Figure 5 shows conversion versus time plots of the fresh and the spent catalysts after four cycles for P.SBA-15SHPd and SiO₂SHPd. The experiments were run at a lower palladium concentration (0.01 mol% of Pd related to iodobenzene). In the case of P.SBA-15SHPd, almost the same reaction rate for fresh and spent catalyst is noted. However, SiO₂SHPd sample displayed a considerable decrease of the reaction rate for the spent catalyst. To reveal the reason for deactivation, the spent catalysts (after four cycles) were studied by X-ray diffraction (XRD) and transmission electron microscopy (TEM). XRD analysis (Figure S4) showed new lines due to changes on enhanced palladium crystallinity for all catalysts, the new pattern lines corresponded to Pd metal with face centered cubic structure. These results differ from Shimizu et al.⁶⁵ which reported no change in palladium crystallinity after the C-C cross coupling reaction using FDU as support. The obtained results give a strong indication that during the catalytic performance the palladium species leached into the solution and were re-deposited on silica surface, leading to particle growth (Ostwald ripening) and enhanced crystallinity of Pd.

TEM analyses of the spent catalysts and histograms of Pd particle size distribution (after 4 cycles) are shown in Figure 6. The structure of Plugged SBA-15 and m-MCF were still recognized, but the palladium particle size had grown slightly, and the majority of metal particles were still found confined in the silica pore structure (Figure 6 B, C). In the case of SiO₂-SHPd, particles grew severely (Figure 6A), very large metal particle from 10-160 nm in diameter were found on the external surface of silica aggregates. These results

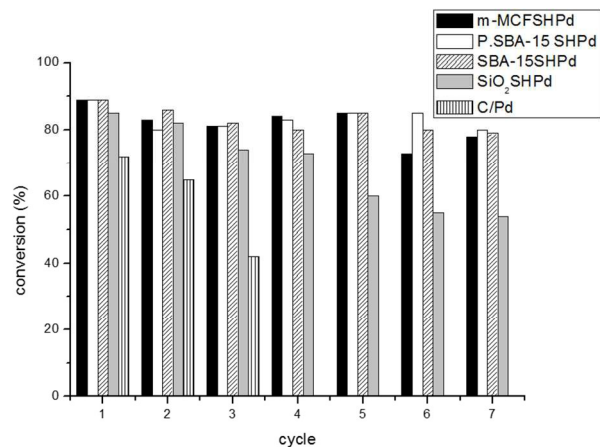


Figure 4 Recyclability of synthesized materials for the Heck reaction

Reaction conditions: 2.25 mmol of iodobenzene, 3.4 mmol of butyl acrylate, 20 mg of supported catalyst (0.13 mol% of palladium), 2.14 mmol of base, 2.0 mL toluene+ 0.2 mL DMF, 100°C, 12 hours (toluene+ DMF)

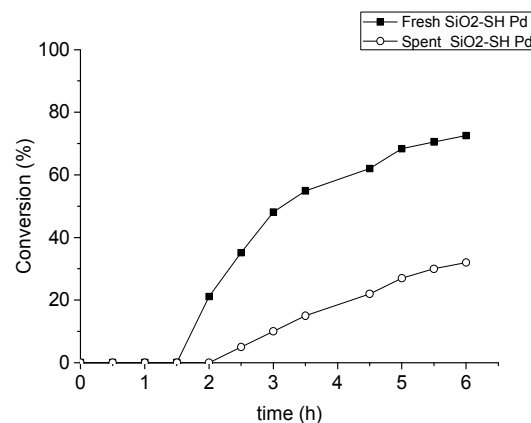
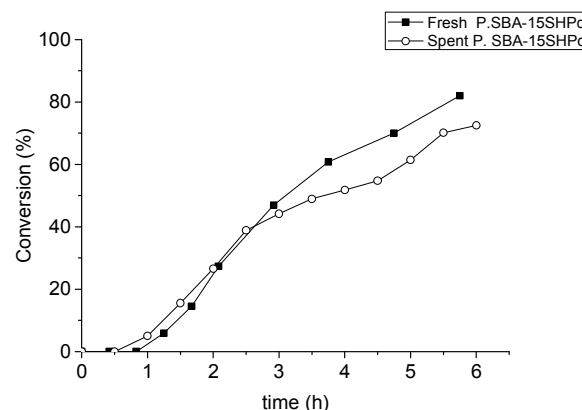


Figure 5 Plot of product yield versus time for the Heck reaction with fresh and spent (after four previous reaction cycles) SiO₂SHPd and P.SBA-15SHPd

Reaction conditions: 22.5 mmol of iodobenzene, 34 mmol of butyl acrylate, 20 mg of supported catalyst (0.01 mol% of palladium), 21.4 mmol of Et₃N, 20 mL toluene+ 2 mL DMF, 100°C

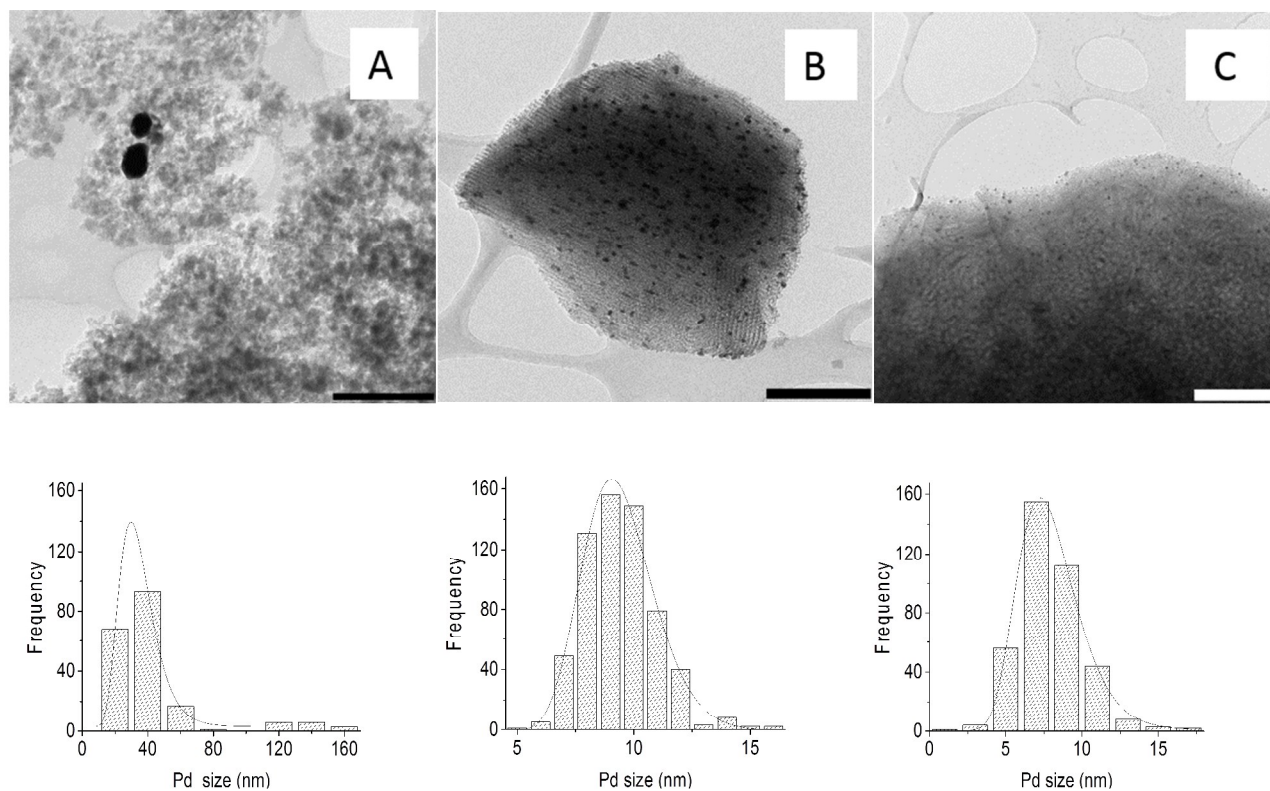


Figure 6 TEM images of spent catalysts after 4th cycle (A) SiO₂-SHPd (B) P.SBA-15SHPd (C) m-MCF SHPd, scale bars 200 nm and derived Pd particle size distributions.

give a strong indication that the combination of thiol groups and confinement of Pd particles in mesopores had restricted the Pd growth in the case of P.SBA-15 and m-MCF, producing more stable catalysts than SiO₂-SHPd where confinement effects were limited. The fact that the great majority of the particles of spent m-MCF SHPd are smaller than particles on spent P-SBA-15SHPd might be related to the small window size of m-MCF limiting the Ostwald ripening.

As shown by hot filtration and PVP test, Pd species leached from the support and brought about the catalytic process in solution. Thus, the recapturing process is very important to reduce the formation of large particles and to extend catalyst life time. Despite having the same density of thiol groups per unit of surface area, the Pd particles grew much more severely on Aerosil, we think that the mesopores of OMM provide a concave surface structure with more effective functionalization and, moreover, the confinement of Pd nanoparticles helps to readsorb Pd species and thereby decrease the palladium particle growth. In the case of Aerosil, the convex surface structure may provide less effective functionalization, on the one hand, and the fact that Pd nanoparticles are not effectively confined inside pores that results in faster growth of Pd particles via Ostwald ripening, on the other hand.

The porosity of spent catalysts was also investigated by N₂ physisorption to examine the stability of OMS under Heck reaction conditions (Figure S6). Isotherms of fresh and spent catalysts showed that the support materials kept the almost same porosity after

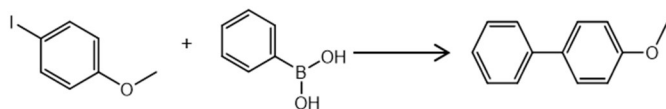
4 cycles, showing no damage to the silica structure under the applied conditions.

The Suzuki reaction

The reaction between 4-iodoanisole and phenylboronic acid was used as a model reaction (Scheme 3). Table 3 shows the performance of P-SBA-15SHPd when different solvents and bases were used. In the case of the Suzuki reaction, Et₃N showed to be inefficient when compared to Na₃PO₄·12H₂O and K₂CO₃. Anhydrous Na₃PO₄ was also used as base, but a lower conversion was observed, indicating the influence of water in this reaction as reported before.⁶⁶ Moreover, ethanol showed to be a better solvent compared to pure DMF and a mixture of DMF and toluene. The conversion of bromide and chloride substrates are shown in Table S4.

The recyclability of the catalysts was carried out using the conditions described in Table 3 entry 7. The commercial Pd/C catalyst was used for comparing its performance with silica-supported catalysts. All catalysts suffered a considerable deactivation after each cycle (Figure 7). SBA-15SHPd suffered the strongest deactivation when compared to the other materials. As observed for the Heck reaction, Pd/C suffered again from severe leaching, leading a short life time.

The stability of the supports was examined to address a possible explanation for this extensive deactivation. Figure 8 shows the low angle XRD pattern for the spent (1 cycle) P-SBA-15SHPd



Scheme 3 The Suzuki reaction between 4-iodoanisole and phenylboronic acid

Table 3 Results of Suzuki reaction of 4-iodoanisole and phenylboronic acid using different bases and solvents for P.SBA-15SHPd

Entry	Solvent	Base	Conversion (%)	T °C
1*	DMF/toluene	Et ₃ N	2	100
2	DMF	Et ₃ N	8	100
3	Ethanol	Et ₃ N	5	60
4	Ethanol	n-butylamine	7	60
5	DMF	Na ₃ PO ₄ ·12H ₂ O	30	60
6	DMF/toluene	Na ₃ PO ₄ ·12H ₂ O	21	60
7	Ethanol	Na ₃ PO ₄ ·12H ₂ O	80	60
8	Ethanol	K ₂ CO ₃	41	60
9	Ethanol	Na ₃ PO ₄	45	60

Conditions: 4-iodoanisole (2.4 mmol), phenylboronic acid (2.88 mmol), base (2.4 mmol), 20 mg of P.SBA-15SHPd (0.12 mol % of Pd), 3 hours. *12 hours

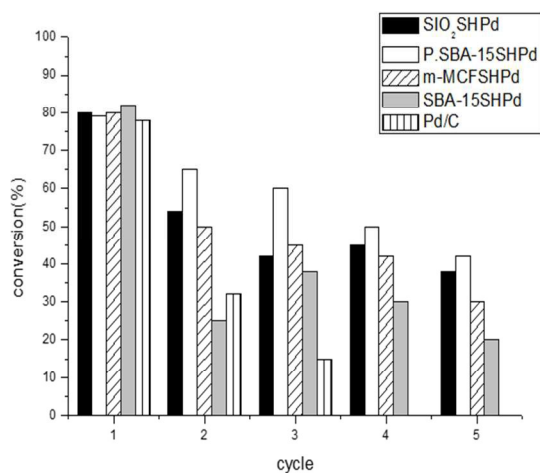


Figure 7 Recyclability of synthesized materials for the Suzuki reaction

Conditions: 4-iodoanisole (2.4 mmol), phenylboronic acid (2.88 mmol), Na₃PO₄·12H₂O (2.4 mmol), around 20 mg of catalyst (0.12 mol % of Pd), 70°C, 3 hours.

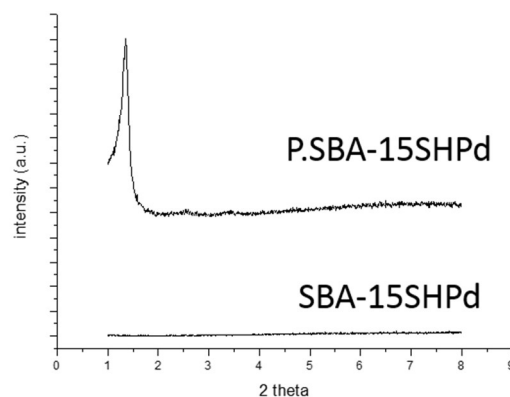


Figure 8 Low angle XRD from SBA-15SHPd and P.SBA-15SHPd used for the Suzuki reaction (after 1st cycle)

and SBA-15SHPd. The peaks which correspond to the *p6mm* configuration are not detected for SBA-15, indicating the pores had collapsed during catalysis. Probably the alkaline condition applied during the Suzuki reaction was responsible for pore collapse. Plugged SBA-15 preserved its structure after the first cycle (Figure 8) as the peaks which correspond to the pore configuration were still visible. This is a clear indication of the higher stability of P-SBA-15 when compared to SBA-15 due to its robust structure and wall thickness. TEM was also used to confirm these results, no well-structured pores were observed on the spent SBA-15 sample, and on the other hand, the pore structure was still observed for P-SBA-15 (Figure S7).

The porosity of spent materials after first cycle was also investigated by N₂ physisorption (isotherms in S.I., S8), all materials faced a strong loss of surface area and pore volume (Table 4). However, plugged SBA-15 showed to be the more resistant material compared to other mesoporous materials SBA-15 and m-MCF. In the case of P.SBA-15, the surface area decreased but not as severe as for SBA-15 and m-MCF, a clear ink-bottle hysteresis could still be seen (S.I, S8). This can also explain the higher metal leaching from

Table 4 Structural characteristic of catalysts after the Suzuki reaction after 1st cycle

Material	BET Surface area (m ² /g)	Pore volume (cm ³ /g)	Pd Leaching (%)*
SBA-15 SHPd	15	0.004	24
P.SBA-15SHPd	154	0.16	5
m-MCFSHPd	50	0.07	15
SiO ₂ SHPd	100	0.16	6

*Based on the original amount of Pd deposited on the silica structure

SBA-15SHPd when compared to SiO₂SHPd and P.SBA-15SHPd (Table 4). Probably the destruction of the pores resulted on the reduction of accessibility of the thiol groups, as a consequence limiting the recovery of the palladium species by the ligands. It is also interesting to point out that P.SBA-15SHPd showed the best recyclability when compared to the other studied supports (Figure 7). For the Suzuki reaction, the collapse of the silica structure might be considered as the main factor for the deactivation of silica-based catalysts. As shown in Table 4, SBA-15 lost 24% of Pd originally deposited on SBA-15, however, the catalyst suffered a larger reduction on activity after the first cycle (from 80% to 26%) which cannot be just explained just by leaching.

CONCLUSION

In summary, the structural stability of Pd species was influenced by the thiol-functionalized silica structure. Here, we report for the first time that for the Heck reaction, the combined effects of functionalization and confinement of Pd nanoparticles in the cavities of ordered mesoporous silica P.SBA-15 or m-MCF was efficient to limit the Ostwald ripening avoiding the formation of large Pd particles that was observed with non-porous silica. Despite having the same Pd particles size distribution, the materials based on OMS showed a better recyclability when compared to non-porous silica due to the prevention of formation of large Pd particles. The hot filtration and PVP tests showed that homogeneous species contributed considerably to the final conversion. Stabilization of heterogeneous Heck Pd catalyst, therefore, cannot be realized by suppression of leaching. Rather, re-adsorption by functionalization in combination with restriction of Pd particle growth by confinement is effective to extend catalyst life time.

In the case of the Suzuki reaction, the use of stronger alkaline conditions promotes a considerable damage to silica supports. This fact resulted in a limited recyclability of all synthesized materials. However, SBA-15 showed to be the most fragile structure, which collapsed during the first cycle, resulting in a poor recyclability when compared to P.SBA-15. The plugs and the most robust structure of P.SBA-15 permitted the material to display a higher stability for the Suzuki reaction, providing an improvement on the recyclability results.

ACKNOWLEDGEMENTS

The authors acknowledge support from European Research Council (ERC) advanced grant no. 338846 and the Dutch National Research School Combination Catalysis (NRSCC).

REFERENCES

1. L.-L. Li, H. Sun, C.-J. Fang, J. Xu, J.-Y. Jin, C.-H. Yan, *J. Mater. Chem.*, 2007, **17**, 4492.
2. R. Métivier, I. Leray, B. Lebeau, B. Valeur, *J. Mater. Chem.*, 2005, **15**, 2965.
3. D.-H. Lin, Y.-X. Jiang, Y. Wang, S.-G. Sun, *J. Nanomater.*, 2008, **2008**, 1.
4. S. Wang, *Micro. Meso. Mater.*, 2009, **117**, 1.
5. I. I. Slowing, J. L. Vivero-Escoto, C.-W. Wu, V. S.-Y. Lin, *Adv. Drug Deliv. Rev.*, 2008, **60**, 1278.
6. M. Vallet-Regí, F. Balas, D. Arcos, *Angew. Chem. Int. Ed. Engl.*, 2007, **46**, 7548.
7. X. Liu, L. Li, Y. Du, Z. Guo, T. T. Ong, Y. Chen, S. C. Ng and Y. Yang, *J. Chromatogr. A*, 2009, **1216**, 7767.
8. H. Wan, L. Liu, C. Li, X. Xue, X. Liang, *J. Colloid Interface Sci.*, 2009, **337**, 420.
9. L. Escamilla-Perea, R. Nava, B. Pawelec, M. G. Rosmaninho, C. L. Peza-Ledesma, J. L. G. Fierro, *Appl. Catal. A Gen.*, 2010, **381**, 42.
10. H. Yang, L. Zhang, W. Su, Q. Yang, C. Li, *J. Catal.*, 2007, **248**, 204.
11. T.-W. Kim, M.-J. Kim, F. Kleitz, M. M. Nair, R. Guillet-Nicolas, K.-E. Jeong, H.-J. Chae, C.-U. Kim, S.-Y. Jeong, *ChemCatChem*, 2012, **4**, 687.
12. M. Shakeri, R. J. M. Klein Gebbink, P. E. de Jongh, K. P. de Jong, *Angew. Chemie*, 2013, **125**, 11054.
13. M. C. G. Albuquerque, I. Jiménez-Urbistondo, J. Santamaría-González, J. M. Mérida-Robles, R. Moreno-Tost, E. Rodríguez-Castellón, A. Jiménez-López, D. C. S. Azevedo, C. L. Cavalcante Jr., P. Maireles-Torres, *Appl. Catal. A Gen.*, 2008, **334**, 35.
14. S. Das, A. Goswami, N. Murali, T. Asefa, *ChemCatChem*, 2013, **5**, 910.
15. A. Taguchi, F. Schüth, *Micro. Meso. Mater.* 2005, **77**, 1.
16. Y.-S. Kim, X.-F. Guo, G.-J. Kim, *Chem. Commun. (Camb.)*, 2009, 4296.
17. H. Yang, L. Zhang, P. Wang, Q. Yang, C. Li, *Green Chem.*, 2009, **11**, 257.
18. H. Yang, X. Han, Z. Ma, R. Wang, J. Liu, X. Ji, *Green Chem.*, 2010, **12**, 441.
19. S.-Y. Chen, T. Yokoi, C.-Y. Tang, L.-Y. Jang, T. Tatsumi, J. C. C. Chan, S. Cheng, *Green Chem.*, 2011, **13**, 2920.
20. J. Fan, X. Jiang, H. Min, D. Li, X. Ran, L. Zou, Y. Sun, W. Li, J. Yang, W. Teng, G. Li, D. Zhao, *J. Mater. Chem. A*, 2014, **2**, 10654.
21. R. L. Oliveira, P. K. Kiyohara, L. M. Rossi, *Green Chem.*, 2010, **12**, 144.
22. R. L. Oliveira, P. K. Kiyohara, L. M. Rossi, *Green Chem.*, 2009, **11**, 1366.
23. Z. Wang, Q. Liu, J. Yu, T. Wu, G. Wang, *Appl. Catal. A Gen.*, 2003, **239**, 87.
24. E. M. Fixman, M. C. Abello, O. F. Gorrioz, L. A. Arrúa, *Appl. Catal. A Gen.*, 2007, **319**, 111.
25. Z. Huang, F. Cui, H. Kang, J. Chen, X. Zhang, C. Xia, *Chem. Mater.*, 2008, **20**, 5090.
26. R. L. Oliveira, D. Zanchet, P. K. Kiyohara, L. M. Rossi, *Chemistry*, 2011, **17**, 4626.
27. Y. Hao, Y. Chong, S. Li, H. Yang, *J. Phys. Chem. C*, 2012, **116**, 6512.
28. G. Prieto, M. Shakeri, K. P. de Jong, P. E. de Jongh, *ACS Nano*, 2014, **8**, 2522.
29. J. Sun, D. Ma, H. Zhang, X. Liu, X. Han, X. Bao, G. Weinberg, N. Pfänder, D. Su, *J. Am. Chem. Soc.*, 2006, **128**, 15756.
30. J. M. Kislner, M. L. Gee, G. W. Stevens, A. J. O. Connor, *Chem. Mater.*, 2003, **15**, 619.
31. H. N. Pham, A. E. Anderson, R. L. Johnson, K. Schmidt-Rohr and A. K. Datye, *Angew. Chem. Int. Ed. Engl.*, 2012, **51**, 13163.
32. P. Van Der Voort, P. I. Ravikovitch, K. P. De Jong, M. Benjelloun, E. Van Bavel, A. H. Janssen, A. V. Neimark, B. M. Weckhuysen, E. F. Vansant, *J. Phys. Chem. B*, 2002, **123**, 5873.
33. P. Van der Voort, P. I. Ravikovitch, K. P. De Jong, a V. Neimark, a H. Janssen, M. Benjelloun, E. Van Bavel, P. Cool, B. M. Weckhuysen, E. F. Vansant, *Chem. Commun. (Camb.)*, 2002, 1010.
34. E. B. Celer, M. Kruk, Y. Zuzek, M. Jaroniec, *J. Mater. Chem.*, 2006, **16**, 2824.
35. M. Shakeri, R. J. M. Klein Gebbink, P. E. de Jongh, K. P. de Jong, *Micro. Meso. Mater.*, 2013, **170**, 340.
36. R. L. Oliveira, M. Shakeri, J. D. Meeldijk, K. P. de Jong, P. E. de Jongh, *Micro. Meso. Mater.*, 2015, **201**, 234.
37. M. Shakeri, L. Roiban, V. Yazerski, G. Prieto, J. M. K. Gebbink, P. E. De Jongh, K. P. De Jong, *ACS Catal.*, 2014, **4**, 3791.
38. F. Yin, S. Ji, P. Wu, F. Zhao, C. Li, *J. Catal.*, 2008, **257**, 108.
39. B. Karimi, S. Abedi, J. H. Clark, V. Budarin, *Angew. Chem. Int. Ed.*, 2006, **45**, 4776.
40. X. Zhang, H. Yin, J. Wang, L. Chang, Y. Gao, W. Liu, Z. Tang, *Nanoscale*, 2013, **5**, 8392.
41. G. Chen, S. Wu, H. Liu, H. Jiang, Y. Li, *Green Chem.*, 2013, **15**, 230-235.
42. P. M. Ulberman, N. J. S. Costa, K. Philippot, R. C. Carmona, A. A. dos Santos, L. M. Rossi, *Green Chem.*, 2014, **16**, 4566.
43. T. Ishida, Y. Onuma, K. Kinjo, A. Hamasaki, H. Ohashi, T. Honma, T. Akita, T. Yokoyama, M. Tokunaga, M. Haruta, *Tetrahedron*, 2014, **70**, 6150.
44. D. D. L. Martins, H. M. Alvarez, L. C. S. Aguiar, O. A. C. Antunes, *Appl. Catal. A Gen.*, 2011, **408**, 47.

- 45.N. J. S. Costa, P. K. Kiyohara, A. L. Monteiro, Y. Coppel, K. Philippot, L. M. Rossi, *J. Catal.*, 2010, **276**, 382.
- 46.D. Das, A. Sayari, *J. Catal.*, 2007, **246**, 60.
- 47.A. Gruber, D. Zim, G. Ebeling, A. Monteiro, J. Dupont, *Org. Lett.*, 2000, **2**, 1287.
- 48.K. Köhler, R. G. Heidenreich, J. G. E. Krauter, J. Pietsch, *Chemistry*, 2002, **8**, 622.
- 49.G. Zhang, H. Zhou, J. Hu, M. Liu, Y. Kuang, *Green Chem.*, 2009, **11**, 1428.
- 50.B. Nohair, S. Macquarrie, C. M. Crudden, S. Kaliaguine, *J. Phys. Chem. C*, 2008, **112**, 6065.
- 51.S. Macquarrie, B. Nohair, J. H. Horton, S. Kaliaguine, C. M. Crudden, *J. Phys. Chem. C*, 2010, **114**, 57.
- 52.M. Pagliaro, V. Pandarus, F. Bèland, R. Ciriminna, G. Palmisano, P. D. Carà, *Catal. Sci. Technol.*, 2011, **1**, 736.
- 53.G. Budroni, a Corma, H. Garcia, A. Primo, *J. Catal.*, 2007, **251**, 345.
- 54.G. Park, S. Lee, S. J. Son, S. Shin, *Green Chem.*, 2013, **15**, 3468.
- 55.J. H. Clark, D. J. Macquarrie, E. B. Mubofu, *Green Chem.*, 2000, **2**, 53.
- 56.B. Karimi, D. Enders, *Org. Lett.*, 2006, **8**, 1237.
- 57.V. Polshettiwar, Á. Molnár, *Tetrahedron*, 2007, **63**, 6949.
- 58.D. Zhang, J. Xu, Q. Zhao, T. Cheng, G. Liu, *ChemCatChem*, 2014, **10**, 2998.
- 59.A. El Kadib, K. McEleney, T. Seki, T. K. Wood, C. M. Crudden, *ChemCatChem*, 2011, **3**, 1281.
- 60.L. Wang, S. Shylesh, D. Dehe, T. Philippi, G. Dörr, A. Seifert, Z. Zhou, M. Hartmann, R. N. Klupp Taylor, M. Jia, S. Ernst, W. R. Thiel, *ChemCatChem*, 2012, **4**, 395.
- 61.L. M. Rossi, L. L. R. Vono, F. P. Silva, P. K. Kiyohara, E. L. Duarte, J. R. Matos, *Appl. Catal. A Gen.*, 2007, **330**, 139.
- 62.R. L. Oliveira, J. B.F. Hooijmans, P.E. deJongh, R. J. M. Klein Gebbink, K. P. de Jong, *ChemCatChem*, 2014,**6**, 3223.
63. X. Ma, Y. Zhou, J. Zhang, A. Zhu, T. Jiang, B. Han, *Green Chem.* 2008, **10**, 59.
64. J. Richardson, C. J. Jones, *Catal.* 2007, **251**, 80.
65. K. Shimizu, S. Koizumi, T. Hatamachi, H. Yoshida, S.Komai, T. Kodama, Y. Kitayama, *J. Catal.* 2004, **228**, 141.
- 66.J. Webb, S. Macquarrie, K. Mceleney, C. Crudden, *J. Catal.*, 2007, **252**, 97.

Notes and references

^a Inorganic Chemistry and Catalysis, Debye Institute for Nanomaterials Science, Utrecht University

^b Organic Chemistry and Catalysis, Debye Institute for Nanomaterials Science, Utrecht University

† Footnotes should appear here. These might include comments relevant to but not central to the matter under discussion, limited experimental and spectral data, and crystallographic data.

Electronic Supplementary Information (ESI) available: [details of any supplementary information available should be included here]. See DOI: 10.1039/b000000x/